EXPLORATORY STUDY ON NEURAL CONTROL OF ROTOR NOISE AND HUB LOADS

Sesi Kottapalli
Aeromechanics Branch
Army/NASA Rotorcraft Division
NASA Ames Research Center
Moffett Field, California

Abstract

Results from an analytical study on simultaneous neural network control of rotor blade vortex interaction (BVI) noise and hub loads are presented in this paper. The present study is an extension of an earlier investigation on neural network identification and control of rotorcraft hub loads. An objective function consisting of the weighted sum of the squares of a four-microphone-average-of-advancing-side-noise and a vibratory-hub-loads-metric was used to characterize the BVI noise and vibratory hub loads. The noise and hub loads data were obtained from a wind tunnel test of a four-bladed rotor with individual blade control during simulated descent. The neural network control procedure was bound by the following ground rules: the controller must converge quickly (in six iterations or fewer) and gradient-based optimization techniques must not be used. A simple iterative procedure for neural control was applied. Two neural networks were used in the procedure requiring a plant model (using a radial-basis function neural network) and separately, an "inverted neural network for control" model (using a back-propagation neural network). A simple calculation that halves the objective function was used in order to speed up convergence. A nonlinear transformation was applied in the reduced data base case in order to make the present neural network control procedure successful for that case as well. For the basic (benchmark) case, the neural network controller successfully achieved simultaneous reductions of 5 dB in the advancing side noise and 54% in the hub loads. Finally, a comparison of the results from the present neural network controller with those from a one-step deterministic controller showed that neural network control was more robust.

Presented at the American Helicopter Society Technical Specialists' Meeting for Rotorcraft Acoustics and Aerodynamics, October 28-30, 1997, Williamsburg, VA.

Notation

A	Rotor disk area, πR^2
A_2	Experimental 2P control amplitude input, deg
$A_{2N,\,i}$	Neural network controller 2P control amplitude input for the i'th iteration, deg
A_{2N}	2P control amplitude input predicted by inverted neural network for control, deg
A_m	Amplitude of mP IBC input, deg
ASNM	Advancing side noise metric, dB
BL-SPL	Band-limited sound pressure level, dB
BVI	Blade vortex interaction
c	Blade chord
C_T	Rotor thrust coefficient, thrust nondimensionalized by $\rho A(\Omega R)^2$
F	Plant model
HHC	Higher Harmonic Control
i	Blade number; i=1 implies ψ=0 for blade at helicopter tail
IBC	Individual Blade Control
INNC	Inverted neural network for control
J	Noise and hub loads objective function, weighted sum of the squares of ASNM and VHLM
J_{BSLN}	Baseline objective function

J_{ND}	Nondimensional objective function, (J/J_{BSLN})
J_T	Transformed (scaled) noise and hub loads objective function, J_{ND}^n
m	Harmonic number for IBC input
MIMO	Multiple-input, multiple-output
MISO	Multiple-input, single-output
Mtip	Rotor tip Mach number
n	Parameter defining J_T, $J_T = J_{ND}^n$
N_b	Number of blades
R	Rotor blade radius
RBF	Radial-basis function
SIMO	Single-input, multiple-output
SISO	Single-input, single-output
SPL	Sound pressure level, dB
[T]	Transfer-function matrix, of size 11 x 2
V	Wind tunnel airspeed, knots
VHLM	Vibratory hub loads metric
$VHLM_{BSLN}$	Vibratory hub loads metric, baseline value
W_{ASNM}	Weight for $ASNM^2$ in objective function J
[W_Z]	Weighting matrix, of size 11 x 11
{ z }	Vector of measured vibratory hub loads (sine and cosine components) and the noise metric, of size 11 x 1
α_s	Rotor shaft angle, positive nose up, deg
{ θ }	Vector of 2P blade pitch control inputs, of size 2 x 1
{ θ^* }	Vector of optimal 2P blade pitch control inputs, of size 2 x 1
θ_{im}	IBC contribution to blade pitch, m'th harmonic pitch for i'th blade
μ	Advance ratio, $V/(\Omega R)$
σ	Rotor solidity, $N_b c/\pi R$
Φ_2	Experimental 2P control phase input, deg
$\Phi_{2N,\,i}$	Neural network controller 2P control phase input for the i'th iteration, deg
Φ_{2N}	2P control phase input predicted by inverted neural network for control, deg
ρ	Air density, $slugs/ft^3$
ψ	Rotor azimuth angle, deg
Ω	Rotor rotational speed, rad/sec

Introduction

The development and implementation of a robust active control system for helicopter aeromechanics must include a method for accurate identification of aircraft parameters and a robust scheme to generate optimal control inputs to best realize a set of objective functions. Specifically, for the aeromechanic problem investigated in this paper, the controller's task would be to first, identify the nonlinear relationship between the rotor induced acoustic and vibration levels, and second, to generate optimal higher harmonic control (HHC) or individual blade control (IBC) pitch control inputs that simultaneously reduce noise and vibration.

As a background to the present neural control study on rotor noise and hub loads, a few relevant studies on the phenomenon of blade vortex interaction (BVI) rotor noise are summarized here. Schmitz (Ref. 1) presents an authoritative, easily readable discussion on rotor noise including BVI noise, and the research studies by Kitaplioglu, et al. (Ref. 2) and McCluer, et al. (Ref. 3) represent recent research.

Rotorcraft advancing side blade vortex interaction noise and vibratory hub loads almost always behave nonlinearly with respect to the phase of an HHC or IBC pitch input.

For rotors with HHC pitch inputs, the noise related nonlinear behavior is evident in wind tunnel test results (Kottapalli, et al., Ref. 4). More recently, noise related nonlinear behavior was observed in wind tunnel test result with IBC pitch inputs (Swanson, et al., Refs. 5 and 6, and Jacklin, et al., Ref. 7).

For rotors with HHC pitch inputs, the hub loads related nonlinear behavior is evident in: wind tunnel test results (Ref. 4); flight test results (Miao, et al., Ref. 8); and analytical results (O'Leary, et al., Ref. 9). More recently, hub loads related nonlinear behavior was observed in wind tunnel test results with IBC pitch inputs (Jacklin, et al., Ref. 7).

Neural network based techniques are attractive nonlinear methods for control of nonlinear systems. Neural networks do not necessarily require large amounts of computational resources or central processor time. Additionally, they appear easy to apply and understand. A successful neural network application enables the accurate identification of important rotorcraft nonlinear parameters and subsequent calculation of the optimal control inputs. An efficient neural network application can enable the hardware implementation of feedback control systems. In the present context, hardware implementation refers to the complete control system and its functions (which includes modeling, predicting, optimizing, and controlling).

The application of neural networks to rotorcraft aeromechanics control is still new; therefore, available literature is limited. For example, in rotorcraft dynamics control, the following literature is available: the 1997 study on identification and control by Kottapalli (Ref. 10), and the 1995 studies on identification by Kottapalli, et al. (Refs. 11 and 12).

However, the following references have been useful for the present investigation. The handbook on intelligent control by White and Sofge (Ref. 13) covers neural control and other approaches. Miller, et al. (Ref. 14), Wasserman (Ref. 15), Werbos (Ref. 16), Omatu (Ref. 17), and Pham and Liu (Ref. 18) discuss various neural control approaches. Werbos (Ref. 16) classifies existing neural control approaches into five types: supervised control systems, direct inverse control, neural adaptive control, back-propagation-through-time, and adaptive critic methods. Other classifications exist (for example, Omatu, et al., Ref. 17). Psaltis, et al. (Ref. 19) discuss architectures associated with training neural networks for neural control. The survey paper by Hunt, et al. (Ref. 20) covers neural networks for control systems. Faller, et al., (Ref. 21) actually consider a fixed-wing aerodynamics application of neural control, namely, real time identification and control of 3-D unsteady separated flow.

The present study is an extension of an earlier investigation on neural network identification and control of rotorcraft hub loads (Ref. 10). The objective of the present study is to develop a robust, neural network based controller to simultaneously minimize advancing side BVI noise and vibratory hub loads. An objective function consisting of the weighted sum of the squares of a four-microphone-average-of-advancing-side-noise and a vibratory-hub-loads-metric was used to characterize the BVI noise and vibratory hub loads. The noise and hub loads data were obtained from a wind tunnel test of a four-bladed rotor with individual blade control during simulated descent. The neural controller is required to be relatively quick in its execution and not be computationally intensive. Thus, the present neural network control procedure is bound by the following ground rules: the controller must converge in six iterations or fewer and gradient-based optimization techniques must not be used.

This study begins with a description of two types of plant models: single-input, single-output (SISO) and single-input, multi-output (SIMO). The SISO model predicts an advancing side noise metric; the SIMO model predicts both the advancing side noise metric and the vibratory hub loads metric. The objective function used in the SIMO application is discussed. Next, the neural network control procedure (based on an existing, neural control technique called the "direct inverse" method, Ref. 15) is described.

The experimental data are then described. Next, five cases are examined. The first four cases pertain to neural control and results are presented in the following sequence: plant model results, inverted neural network for control results, and finally, the neural controller's convergence sequence which includes demonstrated simultaneous control of noise and hub loads. The nonlinear transformation applied in one of the four neural control application cases (the reduced data base case) is discussed. The fifth case looks into the performance of a traditional, one-step deterministic controller and compares its results with those from the neural controller. The fifth case (one-step deterministic controller) includes the first three neural control cases as three, one-step-deterministic-controller subcases. Finally, observations derived from this study are presented.

Plant Model

Kottapalli, et al. (Refs. 11 and 12) have developed procedures for deriving neural network plant models that can be used in the present rotorcraft acoustics and dynamics (controls) application. Single-input, single-output and multiple-input, single-output (MISO) applications were considered in Ref. 11, and the multiple-input, multiple-output (MIMO) application was considered in Ref. 12. Background material on these applications is given in Ref. 11.

In the present study, both SISO and SIMO applications are considered. These plant models are briefly described below.

Single-Input, Single-Output Plant Model

In the SISO application, the network training input is the 2P control phase input Φ_2 where the pitch control amplitude A_2 is maintained at 1.0 deg. The network output is the advancing side noise metric (ASNM) which is discussed as follows.

Advancing Side Noise Metric (ASNM). The present noise metric ASNM was obtained from a four-microphone average of advancing side noise measurements taken during the second U.S./German IBC wind tunnel test (Refs. 5 , 6, and 7). The test article was a four-bladed BO-105 hingeless rotor system. The rotor system was tested in the NASA Ames 40- by 80-Foot Wind Tunnel. Figure 1 (Ref. 5) shows a general layout of the rotor and microphones in the wind tunnel test section. The present ASNM was obtained by taking the average of the noise measurements from microphones 1, 2, 3, and 4 with the traverse location fixed at the advancing side position X = 16.41 ft, Fig. 1. The four sound pressure levels (SPL's) from the microphones were individually summed over the 6th through 40th blade passage frequency band and subsequently averaged to give the present band-limited, sound pressure level based ASNM (BL-SPL ASNM).

Accurate plant modeling in the present SISO application was obtained by using a two-hidden-layer radial basis function (RBF) type of neural network depicted by "1-12-4-1 RBF network." Reference 11 contains more information on how appropriate two-hidden-layered RBF networks are selected as plant models. In the above depiction, the leading and trailing 1's refer to the single input and the single output, and the 12 and 4 refer to the number of processing elements in the first and second hidden layers, respectively.

Single-Input, Multiple-Output Plant Model

The majority of the present neural network results involve the use of the SIMO plant model. In the SIMO application, the network training input is again the 2P control phase input Φ_2 with A_2 = 1.0 deg. The two network outputs are the advancing side noise metric (ASNM) and the vibratory hub loads metric (VHLM). Accurate plant modeling was obtained by using a 1-12-4-2 RBF network.

Objective Function

For the SIMO application, the present study characterizes the advancing side rotor BVI noise and vibratory hub loads by an objective function. The objective function consists of a weighted sum of the squares of a four-microphone-average of advancing side BVI noise and a vibratory hub loads metric:

$$J = (W_{ASNM})\ ASNM^2 + VHLM^2 \qquad (1)$$

where W_{ASNM} is a specified weight. For brevity, the advancing side noise and vibratory hub loads objective function is referred to as the *noise and hub loads objective function.*

The introduction of the noise and hub loads objective function J makes the neural network control procedure developed in Ref. 10 directly applicable to the present noise and hub loads control problem. In the present SIMO application, the objective function J (or the transformed objective function J_T - see Case 4 in Results section) takes the place of the metric VHLM used in Ref. 10.

Neural Network Control Procedure

The present control procedure was finalized after conducting a survey of neural network control techniques and trying several control procedures. In the present SISO and SIMO cases it is possible to obtain accurate modeling and prediction for simulating the plant model being controlled. Therefore, the present control procedure does not include the plant itself. This simplification results in a control procedure that may be classified as "direct control" (Narendra and Parthasarathy, Ref. 22).

A modified version of the "direct inverse control" method in neural control (Wasserman, Ref. 15) is used in this study. This approach is attractive in the present context because of its simplicity and straightforward implementation. This approach does not involve gradient-based optimization techniques. This method assumes that the plant model is invertible, i.e., a unique dependent (y-axis) value exists for a given independent (x-axis) value. Mathematically, Ref. 15 describes the application of the method in the following manner. Let $\mathbf{F}$ be the plant model and $\mathbf{F}^{-1}$ its inverse. The combined system includes the inverse model followed by the plant model. A desired system response that is input to $\mathbf{F}^{-1}$ would ideally give the desired system response as the output of $\mathbf{F}$ since $[\ (\mathbf{F}^{-1})\ \mathbf{F}\ ] = [\ I\ ]$. Therefore, to achieve a desired system output, it is only necessary to provide the specific desired system output as an input (Ref. 15). Without feedback, serious questions can arise regarding the robustness of this method (Ref. 20).

Also, the present plant models (for noise outputs and for combined noise/vibration outputs) are nonlinear and hence noninvertible. Consider the following example. For the linear system y = x, the resulting variation is a straight line; this system is invertible. For the nonlinear system $y = x^2$, the resulting variation is a parabola. This system is noninvertible because when the axes are

inverted, a given "new" x-value does not result in a unique y-value. Recall that the direct inverse control method assumes that the plant model is invertible. The following subsections describe how the presently modified direct inverse control method is applied to rotorcraft acoustics and dynamics controls applications of interest that involve nonlinear (noninvertible) plant models.

The non-feedback direct inverse method is inadequate for general purpose applications. In order to apply the direct inverse control method to the present application, modifications to the method are necessary. Therefore, the present implementation of this method additionally includes an iterative, feedback loop for robustness, and a simple halving technique in order to speed up the neural controller's convergence.

Neural Control Implementation

A block diagram of the present overall neural network control procedure is shown in Fig. 2. For illustrative purposes, this diagram is drawn using the control phase as the relevant feedback parameter. The SIMO case (noise and hub loads objective function) is used as an example in the following description.

In reference to the plant model, the 2P control phase input is the x-axis value, the noise and hub loads objective function is the nonlinear y-axis value. If the axes were to be simply inverted, the noise and hub loads objective function becomes the x-axis value and the 2P control phase input becomes the y-axis value. In this inverted system, a given noise and hub loads objective function does not result in a unique 2P control phase input value (such non-uniqueness has been discussed earlier).

The present control procedure calls only for inverting the axes of the plant model data. This inverted-axes control modeling step "inverts the axes" by using the noise and hub loads objective function as the independent, or input, parameter on the x-axis and the neural network predicted 2P control phase output parameter on the y-axis. Subsequently, an appropriate type of neural network is trained using this inverted-axes data set, thus completing the inverted-axes control modeling step. This step yields a unique x-y relationship corresponding to the input-output relationship of the appropriate neural network. For clarity and brevity, the neural network associated with the inverted-axes control modeling step is referred to as the *inverted neural network for control (INNC).*

The present scheme works for the cases considered because the back-propagation network representing the inverted neural network for control is always able to capture the appropriate functional form of a unique y-axis value for any x-axis value. This is achieved in part since the scheme exploits an artifact of the back-propagation neural network: for extrapolative calculations where training data do not exist, the network output is an approximate average of the existing neighboring data points.

Neural Control Procedure Initiation. Since it is possible to perform accurate identification in the present rotorcraft application, the plant is not included in the neural control procedure ("direct" procedure). The present neural control procedure as outlined in Fig. 2 can be initiated in two ways: 1) inputting a desired noise and hub loads objective function into the inverted neural network for control or 2) inputting a starting value of the control phase input into the plant model. In this study, the neural control procedure was initiated by inputting a 2P control phase input into the plant model.

Neural Control Implementation Details. A simple half-interval calculation which halves the current objective function J (or the transformed objective function - see Case 4 in the Results section) is used at each iterative step (Fig. 2). The iterative control procedure is terminated when the noise and hub loads objective function has converged, that is, has reached a practical global minimum. This approach can also accommodate the application where a desired objective function is specified in advance. This paper does not include results for such an application.

Present Application

Data used in this study were obtained from the second U.S./German Individual Blade Control wind tunnel test (Swanson et al., Refs. 5 and 6, Jacklin, et al., Ref. 7). The test article was a four-bladed BO-105 hingeless rotor system fitted with IBC electro-hydraulic actuators and the test was performed in the NASA Ames 40- by 80-Foot Wind Tunnel, as mentioned earlier.

Four advancing side microphone measurements (Ref. 5) were used in the present study and combined into a single metric by taking their average (giving the present ASNM which is discussed in the section on Plant Model). Five vibratory hub loads (axial, side, and normal forces, and pitching and rolling moments) were obtained (Ref. 7) from the Rotor Test Apparatus steady/dynamic rotor balance in the fixed system. In this study, all loads were referenced to the rotor hub. These loads were combined into a single metric (by taking the square root of the sum of the squares of each load with equal weighting for each load component, giving the metric VHLM).

The test condition considered in the present study is a *high-BVI* condition (Ref. 5). This condition is one of simulated descent at an airspeed of approximately 65 knots ($\mu = 0.15$), Mtip = 0.64, and $C_T/\sigma = 0.075$. Other test parameters are: $\alpha_S = 2.9$ deg, $\Omega = 425$ RPM, with the

hub pitching and rolling moments trimmed to 1600 ft-lb and -350 ft-lb, respectively. This descent condition is equivalent to a 5.6 deg glide slope angle.

The m'th harmonic IBC pitch input for the i'th blade is defined as:

$$\theta_{im} = A_m \sin [m (\psi_i + 90 \text{ deg}) + \Phi_m] \qquad (2)$$

The present application includes five cases and the results from the first four cases help in directly assessing the neural controller's convergence behavior, robustness, and accuracy. The fifth case considers the performance of a traditional, one-step deterministic controller as "re-applied" to the first three cases. The five cases are outlined below.

Case 1. Noise Control: This case considers the variation of the advancing side noise metric with 2P control phase input Φ_2 with a constant control amplitude $A_2 = 1$ deg. The IBC data base for this case has 12 data points ($\Phi_2 = 0$ to 330 deg at 30 deg intervals). During the neural network plant modeling step, periodicity of the metric is ensured by including an additional 13th data point at 360 deg. For this case, the variation of this advancing side noise metric (ASNM) has an ill-defined minimum (Fig. 3). At the same time, for this relatively flat minimum, Φ_2 values between 150 deg and 240 deg are acceptable control inputs that will result in acceptably low advancing side noise levels (Fig. 3). For this case, the neural control procedure is initiated with a 2P control phase input $\Phi_{2N,0} = 0$ deg.

Case 2. Noise and Hub Loads Control: This case is the basic benchmark case, and addresses simultaneous control of advancing side BVI noise and vibratory hub loads. This case considers the variation of the noise and hub loads objective function with 2P control phase input Φ_2 with a constant control amplitude $A_2 = 1$ deg. The IBC data base for this case has 12 data points ($\Phi_2 = 0$ to 330 deg at 30 deg intervals). The advancing side BVI noise metric input data are the same as in Case 1 above, with the vibratory hub loads metric input data being the same as those in Ref. 10. During the neural network plant modeling step, periodicity of the objective function is ensured by including an additional 13th data point at 360 deg. The neural control procedure is initiated with a 2P control phase input $\Phi_{2N,0} = 0$ deg.

Case 3. Starting Point Sensitivity: Using the neural controller from Case 2, a parametric study that assesses the neural controller's robustness is conducted in Case 3. The effect on neural controller convergence of initiating the iterative control procedure using four different starting values of the 2P control phase input (0, 180, 240, and 270 deg) is studied.

Case 4. Reduced Data Base: Here, the Case 2 12-point data set is split into two smaller 6-point data sets based on odd- and even-numbered selections. These two "reduced data base" cases are called Cases 4a and 4b, respectively. Case 4 is important since the results can be used to assess the impact of reducing the number of training data points made available to that part of the neural control procedure which provides an updated estimate of the 2P control phase input.

Case 5. One-Step Deterministic Controller: In addition to the results from the present neural controller, results from a traditional, one-step deterministic controller (Johnson, Ref. 23) were calculated for three cases corresponding to Cases 1, 2 and 3. The one-step deterministic controller cases are called Cases 5a, 5b, and 5c, respectively.

Inverted Neural Network for Control

Depending on the application case under consideration, the network input for the inverted neural network for control (INNC) is as follows:

a. For Case 1 (SISO case), the noise alone is the objective function, and thus the metric ASNM is the network input for INNC.
b. For Cases 2 and 3 (SIMO cases), the combined noise and hub loads objective function J is the network input for INNC.
c. For Case 4 (SIMO case), where a nonlinear transformation is applied to J, the transformed objective function J_T is the network input for INNC.

For all four cases, the network output is the predicted 2P control phase input Φ_{2N}. The inverted neural network for control is trained with 12 input data points in Cases 1 and 2, and six points in Case 4. Overall, the best inverted neural network for control can be determined only after the neural control results for Cases 1 to 4 are computed. At present, the overall conclusion is that a 1-2-3-1 back-propagation neural network can be successfully used as the inverted neural network for control for all the neural control cases considered in this study.

Reference 10 had presented both "small-metric" and "large-metric" results (network outputs) for the inverted neural network for control for which the metric VHLM was the input. In Ref. 10, a large-metric behavior of the desirable type was one that displayed an almost constant value of the 2P control phase input at large values of the input metric. In the present study, depending on the application case, the following "behaviors" corresponding to the "large-metric" behaviors of Ref. 10 are relevant:

a. Case 1: "large ASNM" ("large noise-metric") behavior.
b. Cases 2 and 3: "large J" ("large noise-and-hub-loads-objective-function") behavior.
c. Case 4: "large J_T" ("large transformed-noise-and-hub-loads-objective-function") behavior.

Since in the present study, all of the above three behaviors were of the desirable type, the present study does not present results on these behaviors. Results corresponding to the "small-metric" behavior of Ref. 10 are presented in this study and are as follows:

a. Case 1: "small ASNM" ("small noise-metric") behavior.
b. Cases 2 and 3: "small J" ("small noise-and-hub-loads-objective-function") behavior.
c. Case 4: "small J_T" ("small transformed-noise-and-hub-loads-objective-function") behavior.

Results

The application of neural network control was conducted using the neural networks package NeuralWorks Pro II/PLUS (version 5.2) by NeuralWare (Ref. 24). The Pro II/PLUS package was installed on an ACER Acros personal computer with an Intel 486DX2/66 central processor. All network applications required approximately two minutes of clock time in order to complete the training step.

Results for the neural control cases are presented in the following sequence: plant model results, inverted neural network for control results, and finally, the neural controller's convergence sequence. Results on simultaneous neural control of noise and vibratory hub loads are given in the section on neural controller's convergence.

Case 1. Noise Control

Plant Model. Figure 3 shows the advancing side noise metric's variation with the 2P control phase input Φ_2 for a constant 2P control amplitude $A_2 = 1$ deg. In the figure, the solid circles represent metric values derived from the IBC test data. The baseline (no IBC, $A_2 = 0$ deg) noise metric's value is ASNM = 116 dB (rounded off from 115.5 dB) and the IBC test-based minimum metric's value is ASNM = 108 dB (at $\Phi_2 = 210$ deg). Figure 3 also shows the plant modeling results obtained from the 1-12-4-1 RBF neural network that was trained using 13 input data points. The 1-12-4-1 RBF network was trained for 10,000 iterations; the final RMS error was 0.01.

Inverted Neural Network for Control. The outputs from the 1-2-3-1 back-propagation neural network used as the inverted neural network for control are shown in Fig. 4. This neural network was trained with 12 IBC test data points. The 1-2-3-1 back-propagation network was trained for 20,000 iterations; the final RMS error was 0.50. As can be seen from Fig. 4, the network output is constant, giving a $\Phi_2 = 165$ deg. Unlike the present constant variation in Fig. 4, the inverted neural networks for control that were considered in Ref. 10 were of a shape similar to that of a sigmoid function. In fact, in the present study, the inverted neural network for control results for Cases 2, 3, and 4 all have a sigmoidal shape. The relatively flat, ill-defined minimum that occurs in the variation of Fig. 3 and again, with axes inverted, in Fig. 4 is responsible for the constant network output in the case under consideration, Case 1.

Neural Controller Convergence. For Case 1, due to the constant output of the inverted neural network for control, the converged solution of the neural controller is simply determined by the plant model output for $\Phi_2 =$ 165 deg. The neural controller produces an acceptable, converged minimum noise metric of ASNM = 109 dB where the baseline metric (no IBC, $A_2 = 0$ deg) was 116 dB.

Case 2. Noise and Hub Loads Control

Plant Model. Figure 5 shows the advancing side noise metric and the vibratory hub loads metric on a plot with two vertical axes. These variations are shown with the varying 2P control phase input Φ_2 for a constant 2P control amplitude $A_2 = 1$ deg. In the figure, the solid circles represent the measured advancing side noise metric values and the solid squares represent the measured vibratory hub loads metric values. The baseline (no IBC, $A_2 = 0$ deg) ASNM and VHLM values are 116 dB (Case 1) and 578 (Ref. 10), respectively. The IBC test-based minimum ASNM is 108 dB (at $\Phi_2 = 210$ deg). The IBC test-based minimum VHLM is 211 (at $\Phi_2 = 240$ deg). Figure 5 also shows the plant modeling results obtained from the SIMO 1-12-4-2 RBF neural network that was trained using 13 input data points. The 1-12-4-2 RBF network was trained for 10,000 iterations; the final RMS error was 0.03. This 1-12-4-2 RBF neural network is also used as the plant model in Cases 3 and 4.

Noise and Hub Loads Objective Function: The present noise and hub loads objective function was calculated from Eq. (1) with the weight W_{ASNM} taken as 100, giving:

$$J = (100)\,ASNM^2 + VHLM^2 \qquad (3)$$

Figure 6 shows the resulting noise and hub loads objective function (Eq. 3) using both IBC test data and the SIMO 1-12-4-2 RBF neural network plant model.

W_{ASNM} was selected based on the following reasons. A representative value of the metric-ratio (hub loads metric/noise metric) was used to determine the weight W_{ASNM}. The actual weight used was the square of this ratio in the present quadratic objective function formulation. An example of a representative ratio would be one corresponding to the minimum values of the hub loads and noise metrics. Two other two types of ratios that can be considered are those based on the baseline values of the hub loads and noise metrics, and the maximum values of the hub loads and noise metrics. In other applications, if necessary, representative ratios other than those presently discussed may have to be considered. Based on IBC test data (Fig. 5), the present estimates of the above three metric-ratios are as follows:

Metric-Ratio Type	Metric-Ratio VHLM / ASNM	Metric-Ratio Estimate
Minimum	211 / 108	2
Baseline	578 / 116	5
Maximum	1210 / 118	10

In the present study, the selected metric-ratio was the largest of the above three metric-ratios, namely, 10, giving a weight W_{ASNM} of 100. This weight selection ensures that the noise metric ASNM plays a significant role in the objective function. The present neural network control application, with a weight W_{ASNM} of 100, produced substantial, simultaneous reductions in noise and hub loads (as can be seen from the results of Cases 2, 3, and 4 which are presented as follows).

The IBC test-based baseline value (no IBC input, $A_2 = 0$ deg) of the above combined noise and hub loads objective function (W_{ASNM} =100) was 1.68×10^6 (Fig. 6); with an IBC input of $A_2 = 1$ deg, the minimum value of this objective function occurred at $\Phi_2 = 240$ deg and J was 1.23×10^6.

Figure 6 shows that the present noise and hub loads objective function J does not appear to have a minimum as well-defined as the minimum in the VHLM variation encountered in Ref. 10 (same as the VHLM variation in the present Fig. 5). The VHLM variation (Fig. 5) has two clearly defined minimums, whereas Fig. 6 shows that a relatively flat minimum exists between Φ_2 = 180 and 270 deg for the present objective function.

Inverted Neural Network for Control. The outputs from the 1-2-3-1 back-propagation neural network used as the inverted neural network for control are shown in Fig. 7. This neural network was trained with 12 IBC test data points. The 1-2-3-1 back-propagation network was trained for 20,000 iterations; the final RMS error was 0.27.

Figure 7 shows that the shape of the predicted network output appears to be close to that of a sigmoid function. This could be an attribute of the present inverted neural network for control that is due to an inherent property of the back-propagation neural network. As described in the following section, in general, the above mentioned behavior of the 1-2-3-1 back-propagation neural network is sufficient to make the neural control scheme successful.

Neural Controller Convergence. In the present case, the controller cycle is initiated with a 1 deg 2P control amplitude with phase $\Phi_{2N,\,0} = 0$ deg. Figures 8a and 8b show results from the present neural network controller. The neural controller produces a converged minimum noise and hub loads objective function ($J = 1.30 \times 10^6$) in three iterations (Fig. 8a). The corresponding converged optimal 2P control phase input ($\Phi_{2N,\,3}$) predicted by the neural controller is 240 deg (Fig. 8b).

Figures 9a and 9b show the advancing side noise metric and vibratory hub loads metric corresponding to the 2P control phase input results shown in Fig. 8b. These metrics were obtained by inputting the neural-controller-derived 2P control input value into the SIMO 1-12-4-2 RBF network plant model which outputs the corresponding ASNM and VHLM values. The neural controller produces a converged minimum advancing side noise metric (111 dB) and a converged minimum vibratory hub loads metric (267). Thus, the neural controller is able to achieve simultaneous reductions of 5 dB in the advancing side noise metric and 54% in the vibratory hub loads metric, with respect to the baseline metrics.

Case 3. Starting Point Sensitivity

In Case 3, the starting values of the 2P control phase input $\Phi_{2N,\,0}$ are varied and specified as 0 deg (same as in Case 2), 180, 240, and 270 deg. These values were selected to assess the neural network controller's robustness. The plant model and the inverted neural network for control are the same as those used in Case 2.

Neural Controller Convergence. Figures 10a and 10b show the neural controller convergence sequences for the objective function and the 2P control phase input for the four starting values. Table 1 below shows the corresponding numerical values in which the halving step (Fig. 2) is also noted. The identified halved objective function is the input to the inverted neural network for control at the next iterative cycle. The 240 deg starting point subcase ($\Phi_{2N,\,0} = 240$ deg) required two iterations to converge whereas the other three subcases required three iterations to converge. The objective function

converged to a value of 1.30×10^6 for all four subcases (Fig. 10a). The corresponding predicted, converged 2P control phase input is 240 deg for all four subcases (Fig. 10b).

Figures 11a and 11b show the convergence of the advancing side noise metric and vibratory hub loads metric. The converged values are the same as in Case 2, namely, a converged minimum advancing side noise metric of 111 dB and a converged minimum vibratory hub loads metric of 267. The iterative results are shown in Table 2 and indicate that the present noise and hub loads neural controller is insensitive to a starting point for the current study.

Table 1. Objective Function Starting Point Sensitivity, Neural Control

Iteration No.	2P control phase input into PM deg	Identified/ Halved Object. Funct. ($\times 10^{-6}$)	2P control phase input from INNC deg
Starting Point = 0 deg			
0	0	2.48/1.24	237
1	237	1.30/0.65	240
2	240	1.30/0.65	240
3	240	1.30	
Starting Point = 180 deg			
0	180	1.45/0.72	240
1	240	1.30/0.65	240
2	240	1.30/0.65	240
3	240	1.30	
Starting Point = 240 deg			
0	240	1.30/0.65	240
1	240	1.30/0.65	240
2	240	1.30	
Starting Point = 270 deg			
0	270	1.41/0.70	240
1	240	1.30/0.65	240
2	240	1.30/0.65	240
3	240	1.30	

(PM: plant model, INNC: inverted neural network for control)

Case 4. Reduced Data Base

This case has two subcases, Cases 4a and 4b. During the inverted neural network for control modeling step, these two subcases use two different "reduced data base" 6-point training data sets. In Case 4a, the six odd-numbered training points from the original 12-point training data set (IBC test data) are used; similarly, in Case 4b the six even-numbered points are used. The plant models for Cases 4a and 4b are the same as those used in Case 2 (13-point training data set).

Table 2. Noise and Hub Loads Starting Point Sensitivity, Neural Control

Iteration No.	2P control phase input into PM deg	Identified ASNM/ VHLM
Starting Point = 0 deg		
0	0	109 dB / 1132
1	237	110 dB / 289
2	240	111 dB / 267
3	240	111 dB / 267
Starting Point = 180 deg		
0	180	109 dB / 512
1	240	111 dB / 265
2	240	111 dB / 267
3	240	111 dB / 267
Starting Point = 240 deg		
0	240	111 dB / 267
1	240	111 dB / 267
2	240	111 dB / 267
Starting Point = 270 deg		
0	270	117 dB / 218
1	240	111 dB / 265
2	240	111 dB / 267
3	240	111 dB / 267

(PM: plant model)

Objective Function Transformation. The variation of the present noise and hub loads objective function with the 2P control phase input Φ_2 does not have a clearly defined minimum (Fig. 6); instead, a relatively flat trend exists in this variation between Φ_2 = 180 and 270 deg (Fig. 6). Also, unlike the simpler application considered in Ref. 10, which involved inverted neural network for control x-axis inputs of the order of 10^3, the present application involves inverted neural network for control x-axis inputs of the order of 10^6. In order to obtain *simultaneous reductions* in the advancing side noise metric and the vibratory hub loads metric in the present reduced data base cases, a nonlinear transformation (scaling) of the objective function was introduced. Without such a transformation, the output variations of the inverted neural networks for control for the "untransformed" reduced data base cases are not "well

behaved": that is, their extrapolated segments (Φ_{2N} values near J = 0) were not able to produce simultaneous reductions in noise and hub loads.

In order to obtain well-behaved outputs of the inverted neural network for control with the goal of producing simultaneous noise and hub loads reductions, the following two steps were introduced for Case 4, the Reduced Data Base case:

1. The objective function J was divided by its baseline value giving the nondimensional objective function $J_{ND} = (J/J_{BSLN})$. This step precludes the occurrence of any problems that could arise due to the objective function being of the order of 10^6. However, the immediate consequence from this step is that a nondimensional noise and hub loads objective function is more amenable to subsequent transformation since it is of the order of 1 (10^0).

2. An appropriate transformation that would make the nondimensional objective function J_{ND} variation less flat was introduced. Subsequent to such a transformation, values of J_{ND} less than one would get smaller and values of J_{ND} greater than one would get larger. The transformed objective function variation (J_T) produces well-behaved inverted neural network for control outputs (Case 4).

The presently transformed noise and hub loads objective function J_T is given as follows:

$$J_T = J_{ND}^n = (J/J_{BSLN})^n \qquad n > 1 \qquad (4)$$

The parameter "n" was determined in the present case by making the minimum value of the present $J_T = (J/J_{BSLN})^n$ (at $\Phi_2 = 240$ deg) approximately the same (or smaller) as the minimum value of the nondimensional ratio ($VHLM/VHLM_{BSLN}$) (also at $\Phi_2 = 240$ deg) that was encountered in the successful vibratory hub loads application considered in Ref. 10. This is shown as follows:

n	Min. $VHLM/VHLM_{BSLN}$	Min. J_T
1	0.37	0.74
2	0.37	0.54
3	0.37	0.40
4	0.37	0.29

In the present study, the parameter "n" was selected as 4. Figure 12 shows the variations of the transformed objective function J_T and the unscaled, nondimensional J_{ND}. The two 6-point data bases required in Cases 4a and 4b were selected from the 12-point J_T data base. In the present overall neural network control procedure (Fig. 2), the quantity that is actually input to the Case 4 inverted neural network for control is the halved value given as follows: $[(J/2)/J_{BSLN}]^4$.

Case 4a. Odd-Numbered, Six Point Data Base

Inverted Neural Network for Control: Figure 13 shows the output of the 1-2-3-1 back-propagation neural network used as the inverted neural network for control. This network was trained using the odd-numbered six point data base. The 1-2-3-1 back-propagation network was trained for 20,000 iterations; the final RMS error was 0.23. Figure 13 shows that the appropriate functional form for the output of the inverted neural network for control can be generated from six, odd-numbered training points instead of the baseline twelve points (Fig. 7).

Neural Controller Convergence: The controller iterations were initiated with a 1 deg control amplitude with a starting 2P control phase $\Phi_{2N,\,0} = 0$ deg. Figure 14a shows that the present neural controller converges in three iterations to a value of $J = 1.32 \times 10^6$. Figure 14b shows that the corresponding converged optimal 2P control phase input $\Phi_{2N,\,3}$ predicted by the neural controller is 248 deg. This compares favorably to a converged J of 1.30×10^6 at a 2P control phase input of 240 deg from Cases 2 and 3.

Figures 15a and 15b show the advancing side noise metric and the vibratory hub loads metric corresponding to the 2P control phase input results shown in Fig. 14b. The converged advancing side noise metric ASNM was 112 dB and the vibratory hub loads metric VHLM was 228. For the odd-numbered, six-point case, the present noise and hub loads neural controller was able to achieve simultaneous reductions of 3 dB (taking into account round-off error) in the advancing side noise metric and 61% in the vibratory hub loads metric.

Case 4b. Even-Numbered, Six Point Data Base

Inverted Neural Network for Control: Figure 16 shows the output of the 1-2-3-1 back-propagation neural network used as the inverted neural network for control. This network is trained using the even-numbered six point data base. The 1-2-3-1 back-propagation network was trained for 20,000 iterations; the final RMS error was 0.26. Figure 16 shows that the appropriate functional form can be generated from six, even-numbered training points instead of the baseline twelve points (Fig. 7).

Neural Controller Convergence: The controller iterations were initiated with a 1 deg 2P control

amplitude with a starting 2P control phase $\Phi_{2N,\,0} = 0$ deg. Figure 17a shows that the present neural controller converges in three iterations to an objective function J of 1.30×10^6. Figure 17b shows that the corresponding converged optimal 2P control phase input $\Phi_{2N,\,3}$ predicted by the neural controller is 233 deg.

Figures 18a and 18b show the advancing side noise metric and the vibratory hub loads metric corresponding to the 2P control phase input results shown in Fig. 17b. The corresponding converged advancing side BVI noise metric ASNM was 110 dB and the vibratory hub loads metric VHLM was 317. For the even numbered, six-point case, the present neural controller was able to achieve simultaneous reductions of 6 dB in the advancing side noise metric and 45% in the vibratory hub loads metric.

The preceding results from Cases 1 to 4 indicate that the inverted neural network for control modeling step is sufficiently robust and accurate for the present neural control purposes involving control of noise and hub loads.

Case 5. One-Step Deterministic Controller

Using linear transfer-function identification theory and the quadratic performance function formulation (Johnson, Ref. 23), the performance of a one-step deterministic controller is assessed in Case 5.

Linear Transfer-Function Matrix Identification. The vector of responses (advancing side noise metric and the vibratory hub loads) is assumed to vary linearly with the control input as given below:

$$\{ z \} = [T] \{ \theta \}$$

Here, $\{ z \}$ is the response vector, $[T]$ is the linear transfer-function matrix, and $\{\theta \}$ is the control input vector. In the present case, the vectors $\{ z \}$ and $\{ \theta \}$ are made up of the experimental advancing side noise metric and the vibratory hub load components, and 2P control sine and cosine phase inputs, respectively. For present implementation purposes, the original (Ref. 10) response vector $\{ z \}$ (with 10 elements corresponding to the 10 vibratory hub loads components), was augmented by including the noise metric as the 11th element, thus giving the present response vector $\{ z \}$ with 11 elements.

The present one-step deterministic controller applications include one advancing side noise metric (average) and ten vibratory hub load components (sine and cosine components of five hub load components). Separate single harmonic sine and cosine least-square fits from twelve measurements (2P control phase input varying from 0 deg to 330 deg in 30 deg increments) are used to determine the elements of the T-matrix.

Optimal One-Step Deterministic Control Input. The optimal control input is calculated based on a quadratic performance function with the advancing side noise metric weighted 100 times more than the vibratory hub loads components, with all vibratory hub loads responses equally weighted. The performance function is defined as follows:

$$J = \{ z \}^T [W_Z] \{ z \}$$

For the present one-step deterministic controller, the optimal control input vector is calculated using Eq. A1 (Appendix). In Eq. A1, the 2 x 1 vector of optimal control inputs $\{ \theta^* \}$ consists of the sine and cosine components from which the 2P control optimal phase input is calculated. In the following, the subscript "s" refers to the starting condition for the one-step deterministic controller.

Case 5a. Noise Control: This case involves the advancing side noise variation only, Fig. 3. A single harmonic sine and cosine least-square fit was used to determine the best 2P control phase input, and the resulting value was 140 deg. With this 2P control phase input of 140 deg, the SISO 1-12-4-1 RBF plant model gave an advancing side noise metric of 110 dB. For purposes of comparison, the neural network control results for the corresponding case (Case 1) were as follows: a 2P control phase input of 165 deg and a corresponding advancing side noise metric of 109 dB.

Case 5b. Baseline Results: In Case 5b, the starting condition is the baseline condition: $\{ \theta \}_S = \{ 0 \}$ deg (no IBC, $A_2 = 0$ deg), and with the starting response vector $\{ z \}_S$ taken as the baseline experimental advancing side noise metric and hub loads vector (ten vibratory hub load sine and cosine components). Here, ASNM and VHLM are calculated using the plant model of Case 2 and requiring that the 2P control amplitude input is 1 deg .

For Case 5b, the present one-step, noise and hub loads deterministic controller predicts an optimal 2P control phase input of 207 deg. Using the SIMO 1-12-4-2 RBF plant model, the corresponding advancing side noise metric was calculated to be 107 dB and the vibratory hub loads metric was 507. For purposes of comparison, the neural network control results of Cases 2 and 3 were as follows: a converged 2P control phase input of 240 deg, and a corresponding advancing side noise metric of 111 dB and a vibratory hub loads metric of 267. The present observation is that the two control methods give different minimums. The one-step deterministic controller gives an "acoustic" solution in which only the noise is reduced with a small reduction in the vibration. The neural controller simultaneously controls both acoustic and

vibration levels, with substantial reductions in both. Note that the starting conditions are different for these two methods: the one-step deterministic controller starts out with the baseline condition whereas the neural controller starts out with a non-zero 2P control phase input.

Case 5c. Starting Point Sensitivity: In Case 5c, each of the four sets of $\{ \theta \}_S$ and $\{ z \}_S$ vectors is separately determined by the following four 2P control phase input values: 0, 180, 240, and 270 deg , each with $A_2 = 1$ deg . The control input vector $\{ \theta \}_S$ is directly obtained from the 2P control phase input under consideration, and the starting response vector $\{ z \}_S$ is taken as the experimental advancing side noise metric and the hub loads vector corresponding to the particular 2P control phase input under consideration. The table below shows the results of the sensitivity study which evaluates the performance of the one-step deterministic controller performance for the four starting points.

The "starting point sensitivity" one-step deterministic controller results shown in Table 3 below can be compared to those from the neural controller (Case 3, Table 2). This comparison shows that for advancing side noise and vibratory hub loads control, the two control methods can give different solutions, with neural control being more robust. The one-step deterministic controller yields relatively poor simultaneous reductions for the 270 deg starting condition (ASNM = 108 dB and VHLM = 533, as obtained from the SIMO 1-12-4-2 RBF plant model) as compared to the corresponding neural network result (Table 2, ASNM = 111 dB, VHLM = 267).

Table 3. Starting Point Sensitivity, One-Step Deterministic Control, $A_2 = 1$ deg

Starting 2P control phase input deg	Predicted ASNM/ VHLM	Predicted 2P control phase input deg
0	111 dB / 253	242
180	112 dB / 243	244
240	111 dB / 270	240
270	108 dB / 533	195

Concluding Remarks

The application of neural networks to simultaneous control of rotorcraft acoustics and dynamics is new. The objective of the present study was to develop a robust neural-network-based controller to simultaneously minimize BVI noise and vibratory hub loads. An objective function consisting of the weighted sum of the squares of a four-microphone-average-of-advancing-side-BVI-noise and a vibratory-hub-loads-metric was used to characterize the rotor BVI noise and vibratory hub loads. The noise and hub loads data were obtained from a wind tunnel test of a four-bladed rotor with individual blade control during simulated descent. The present neural network control procedure was bound by the following ground rules: the controller must converge in six iterations or fewer and gradient-based optimization techniques must not be used.

A simple iterative procedure for neural control was applied. Two neural networks were used in the procedure requiring a plant model (using a radial-basis function neural network) and separately, an inverted neural network for control model (using a back-propagation neural network). A nonlinear transformation was applied in the reduced data base case in order to make the present neural network control procedure successful for this case as well. The training of each network required approximately two minutes of clock time. Within the overall, iterative neural network control procedure, a simple calculation which halves the noise and vibratory hub loads objective function was used in order to speed up convergence.

The neural network controller was successful in achieving convergence within a limited number of iterations while being robust and computationally efficient.

Four neural network control cases and a single, one-step deterministic control application case were considered in this study. The cases involved variation in the individual blade control 2P control phase input (2P control amplitude fixed). Specific findings from the present study were as follows:

1. The present study showed that simultaneous neural network control of advancing side blade vortex interaction noise and vibratory hub loads can be considered in the same overall manner as neural network control of only vibratory hub loads.

2. In order to obtain simultaneous reduction of advancing side blade vortex interaction noise and vibratory hub loads in the neural network *reduced data base case*, it was necessary to introduce a nonlinearly transformed objective function to obtain an appropriate inverted neural network for control.

3. The present neural network controller successfully achieved the objective of simultaneous, substantial reductions in advancing side blade vortex interaction noise (5 dB reduction) and in vibratory hub loads

(54% reduction) within six iterations without using gradient-based optimization techniques.

4. Results from the four neural control cases showed that the present neural network control procedure is robust.

5. A comparison of the results from the present neural controller with those from a one-step deterministic controller showed that the two control methods can give different solutions, with neural control being more robust.

Acknowledgments

The author wishes to thank Donald Soloway and Chuck Jorgensen (NeuroEngineering Group, Computational Sciences Division, NASA Ames) for their invaluable help.

References

1. Schmitz, F.H., "Rotor Noise," Aeroacoustics of Flight Vehicles: Theory and Practice, Volume 1: Noise Sources, edited by Hubbard, H.H., NASA Reference Publication 1258, Vol. 1, WRDC Technical Report 90-3052, 1991.

2. Kitaplioglu , C., Caradonna, F.X., and Burley, C.L., "Parallel Blade-Vortex Interactions: An Experimental Study and Comparison with Computations," American Helicopter Society Second International Aeromechanics Specialists Conference, Bridgeport, Connecticut, October 1995.

3. McCluer, M., Baeder, J.D., and Kitaplioglu, C., "Comparison of Experimental and Blade-Vortex Interaction Noise with Computational Fluid Dynamic Calculations," American Helicopter Society 51st Annual Forum, Fort Worth, Texas, May 1995.

4. Kottapalli, S., Swanson, S., LeMasurier, P., and Wang, J., "Full-Scale Higher Harmonic Control Research to Reduce Hub Loads and Noise," American Helicopter Society 49th Annual Forum, St. Louis, Missouri, May 1993.

5. Swanson, S., Jacklin, S.A., Blaas, A., Niesl, G., and Kube, R., "Acoustic Results from a Full-Scale Wind Tunnel Test Evaluating Individual Blade Control," American Helicopter Society 51st Annual Forum, Fort Worth, Texas, May 1995.

6. Swanson, S., Jacklin, S.A., Blaas, A., Kube, R., and Niesl, G., "Individual Blade Control Effects on Blade-Vortex Interaction Noise," American Helicopter Society 50th Annual Forum, Washington, D.C., May 1994.

7. Jacklin, S., Blaas, A., Kube, R., and Teves, D., "Reduction of Helicopter BVI Noise, Vibration, and Power Consumption through Individual Blade Control," American Helicopter Society 51st Annual Forum, Ft. Worth, Texas, May 1995.

8. Miao, J., Kottapalli, S.B.R., and Frye, H.M., "Flight Demonstration of Higher Harmonic Control (HHC) on S-76," American Helicopter Society 42nd Annual Forum, Washington, D.C., June 1986.

9. O'Leary, J.J., Kottapalli, S.B.R., and Davis, M., "Adaptation of a Modern Medium Helicopter (Sikorsky S-76) to Higher Harmonic Control," 2nd Decennial Specialists Meeting on Rotorcraft Dynamics, NASA Ames Research Center, Moffett Field, California, November 1984.

10. Kottapalli, S., "Identification and Control of Rotorcraft Hub Loads Using Neural Networks," American Helicopter Society 53rd Annual Forum, Virginia Beach, Virginia, April-May 1997.

11. Kottapalli, S., Abrego, A., and Jacklin, S., "Application of Neural Networks to Model and Predict Rotorcraft Hub Loads," American Helicopter Society Second International Aeromechanics Specialists Conference, Bridgeport, Connecticut, October 1995.

12. Kottapalli, S., Abrego, A., and Jacklin, S., "Multiple-Input, Multiple-Output Application of Neural Networks to Model and Predict Rotorcraft Hub Loads," Sixth International Workshop on Dynamics and Aeroelastic Stability of Rotorcraft Systems, Los Angeles, California, November 1995.

13. Handbook of Intelligent Control (Neural, Fuzzy, and Adaptive Approaches), edited by White, D. A. and Sofge, D.A., Van Nostrand Reinhold, New York, 1992.

14. Neural Networks for Control, edited by Miller, W.T., Sutton, R.S., and Werbos, P.J., The MIT Press, Cambridge, Massachusetts, 1990.

15. Advanced Methods in Neural Computing, Wasserman, P.D., Van Nostrand Reinhold, New York, 1993.

16. Werbos, P.J., "Neurocontrol and Supervised Learning: An Overview and Evaluation," Handbook of Intelligent Control (Neural, Fuzzy, and Adaptive Approaches), edited by White, D. A. and Sofge, D.A., Van Nostrand Reinhold, New York, 1992.

17. Neuro-Control and its Applications, Omatu, S., Khalid, M., and Yusof, R., Advances in Industrial Control, Springer, 1996.

18. Neural Networks for Identification, Prediction and Control, Pham, D.T. and Liu, X., Springer, 1995.

19. Psaltis, D., Sideris, A., and Yamamura, A.A., "A Multilayered Neural Network Controller," *IEEE Control Systems Magazine*, April 1988.

20. Hunt, K.J., Sbarbaro, D., Zbokowski, R, and Gawthrop, P.J., "Neural Networks for Control Systems-A Survey," *Automatica,* Vol. 28, No. 6, 1992, pp. 1083-1112.

21. Faller, W.E., Schreck, S.J., and Lutges, M.W., "Real-Time Prediction and Control of Three-Dimensional Unsteady Separated Flow Fields Using Neural Networks," AIAA Paper 94-0532, 32nd Aerospace Sciences Meeting & Exhibit, Reno, Nevada, January 1994.

22. Narendra, K.S. and Parthasarathy, K., "Identification and Control of Dynamical Systems Using Neural Networks," *IEEE Transactions on Neural Networks*, Vol. 1 (1), March 1990, pp. 4-27.

23. Johnson, W., "Self-Tuning Regulators for Multicyclic Control of Helicopter Vibration," NASA Technical Paper 1996, March 1982.

24. NeuralWorks Manuals:
    a. Reference Guide
    b. Neural Computing
    c. Using NeuralWorks

NeuralWare, Inc., Pittsburgh, Pennsylvania, 1995.

Appendix

One-Step Deterministic Controller Equations
Noise and Hub Loads

Optimal Control Input

The optimal one-step deterministic controller control input vector used in the present study is derived as follows. From Johnson (Ref. 23), the optimal control input is:

$$\{ \theta^* \}_n = [C] (\{ z \}_{n-1} - [T] \{ \theta \}_{n-1})$$

where the subscript "n" refers to a time step and the controller gain [C] is given by:

$$[C] = - ([T]^T [W_Z] [T])^{-1} [T]^T [W_Z]$$

where [W_Z] is the weighting matrix consisting of the weights for the noise metric and the hub loads (sine and cosine components).

The optimal control input equation is presently used in the following manner in order to calculate the optimal one-step control input vector:

$$\{ \theta^* \} = [C] (\{ z \}_S - [T] \{ \theta \}_S) \qquad \text{(A1)}$$

where the subscript "s" refers to the one-step starting condition.

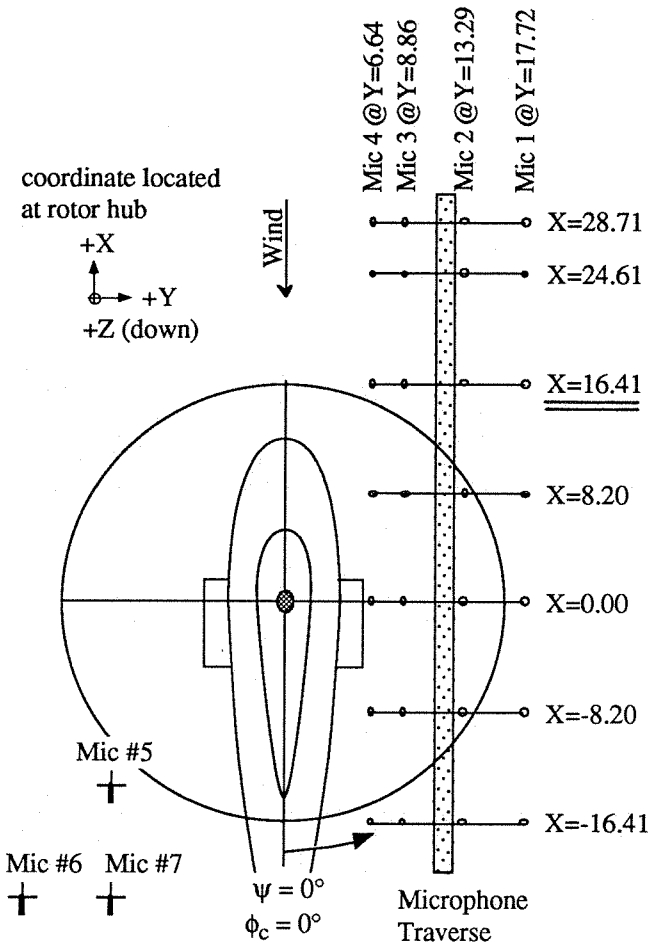

Fig. 1 General layout of rotor and microphones in wind tunnel test section (Swanson, et al., Ref. 5)

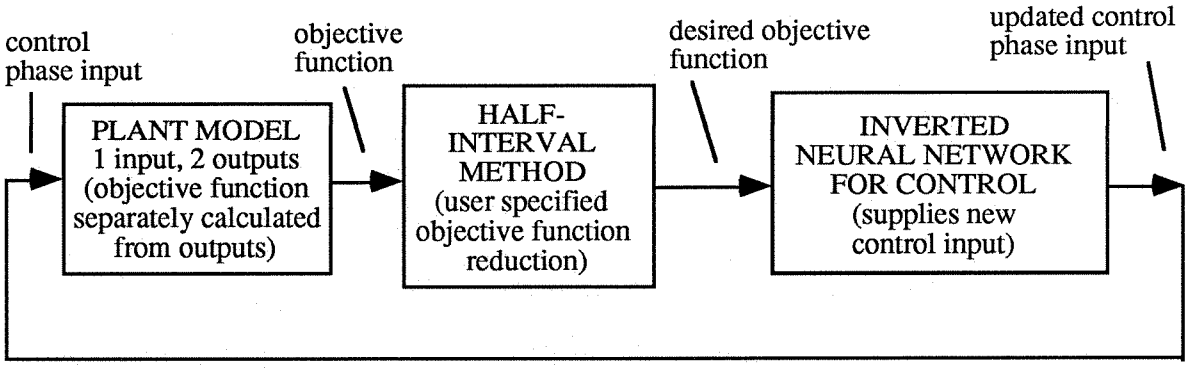

Fig. 2. Overall neural network control procedure for reducing noise and hub loads.

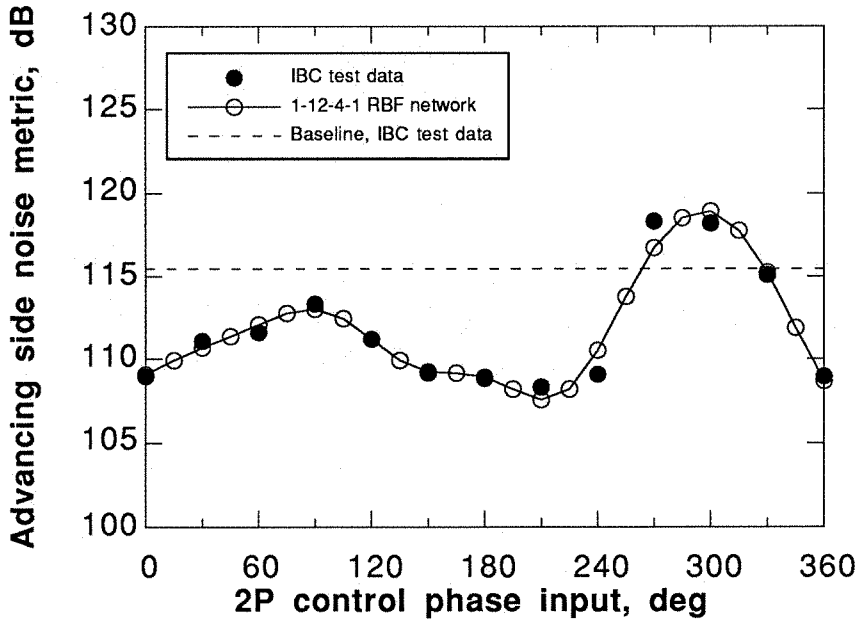

Fig. 3. Case 1 (Noise Control) Experimental noise metric and plant modeling by neural network

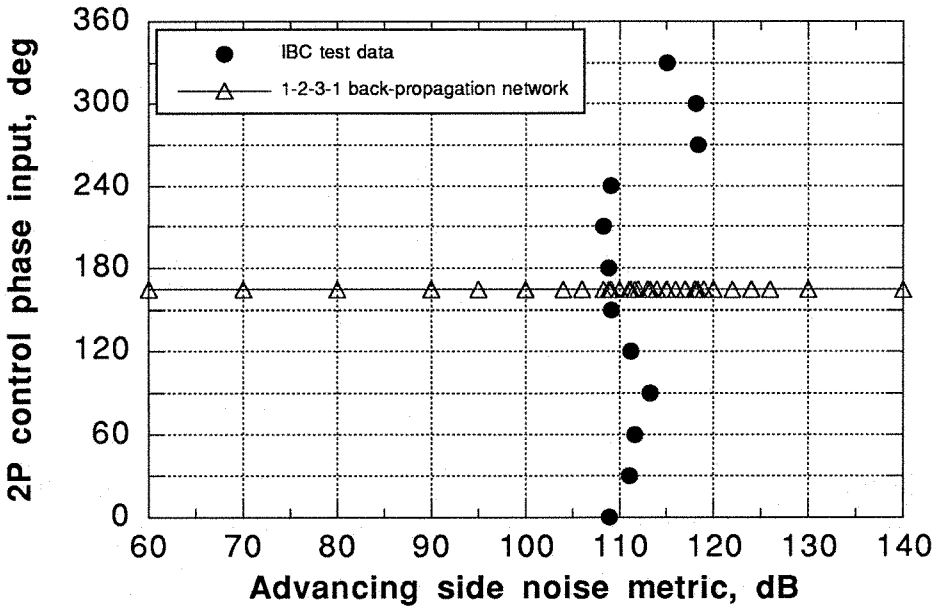

Fig. 4 Case 1 (Noise Control), output of inverted neural network for control, 12 training points.

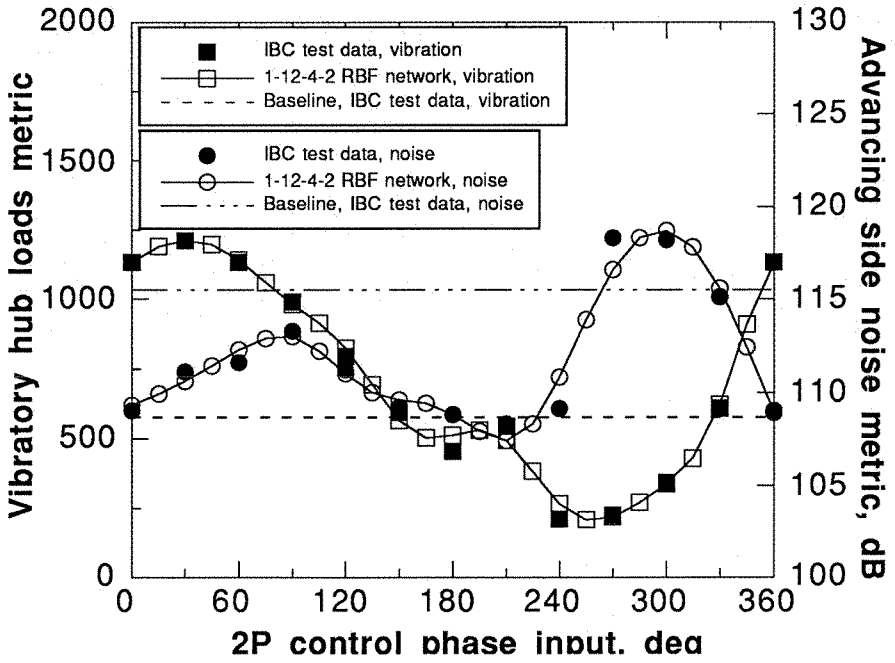

Fig. 5. Case 2 (Noise and Hub Loads Control), noise metric and hub loads metric.

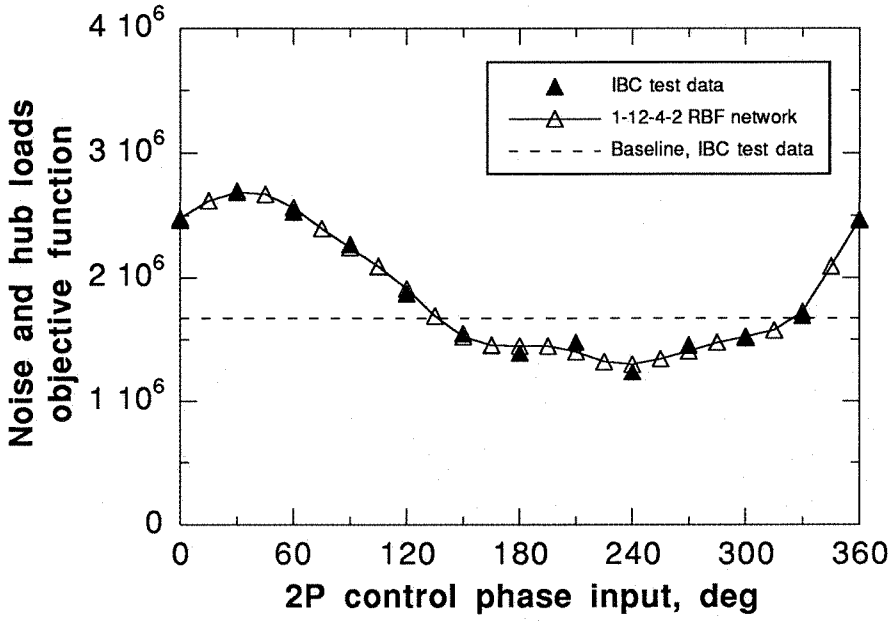

Fig. 6 Case 2 (Noise and Hub Loads Control), noise and hub loads objective function.

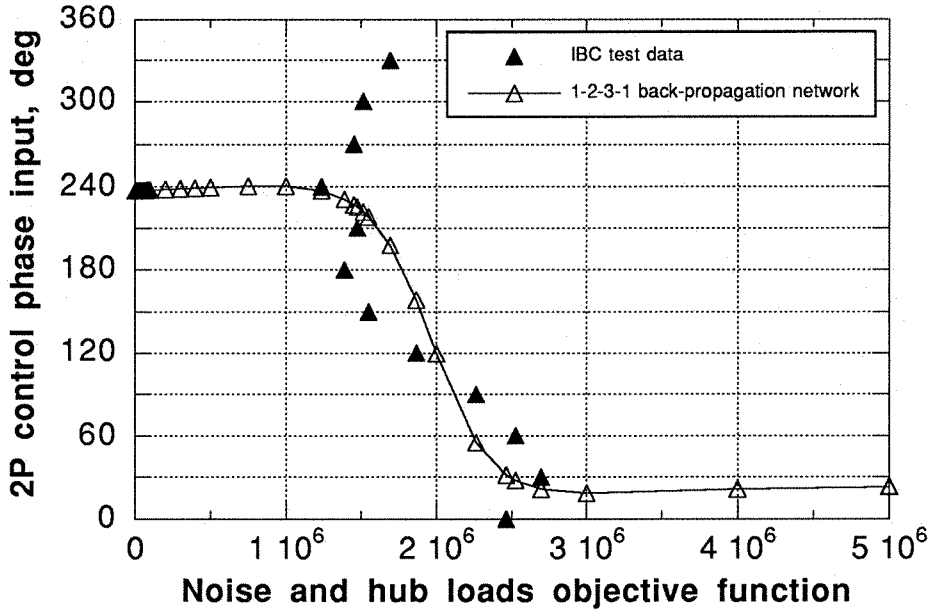

Fig. 7. Case 2 (Noise and Hub Loads Control), output of inverted neural network for control, 12 training points.

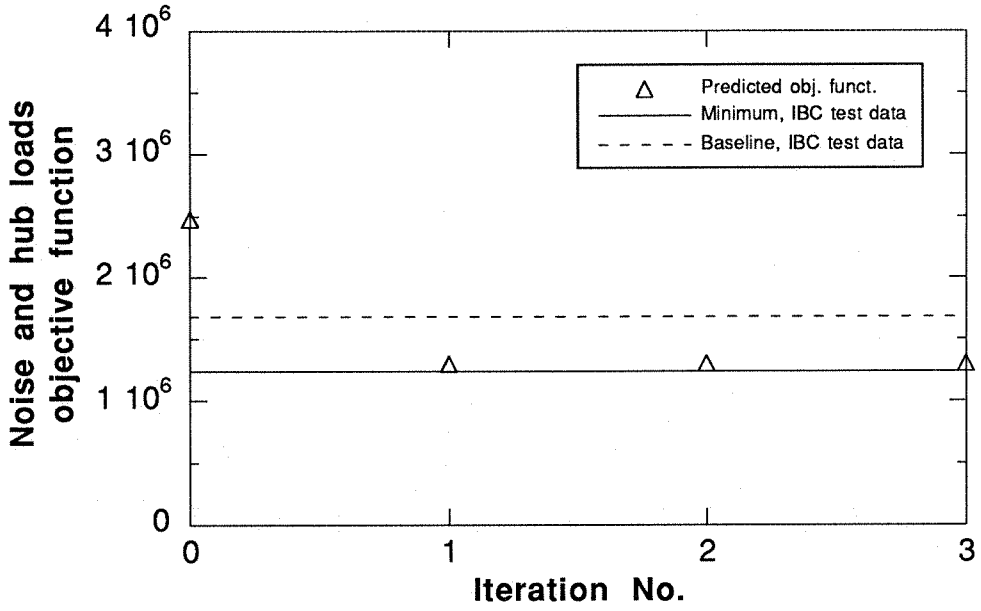

Fig. 8a. Case 2 (Noise and Hub Loads Control), convergence of objective function J (simultaneous neural control of noise and hub loads).

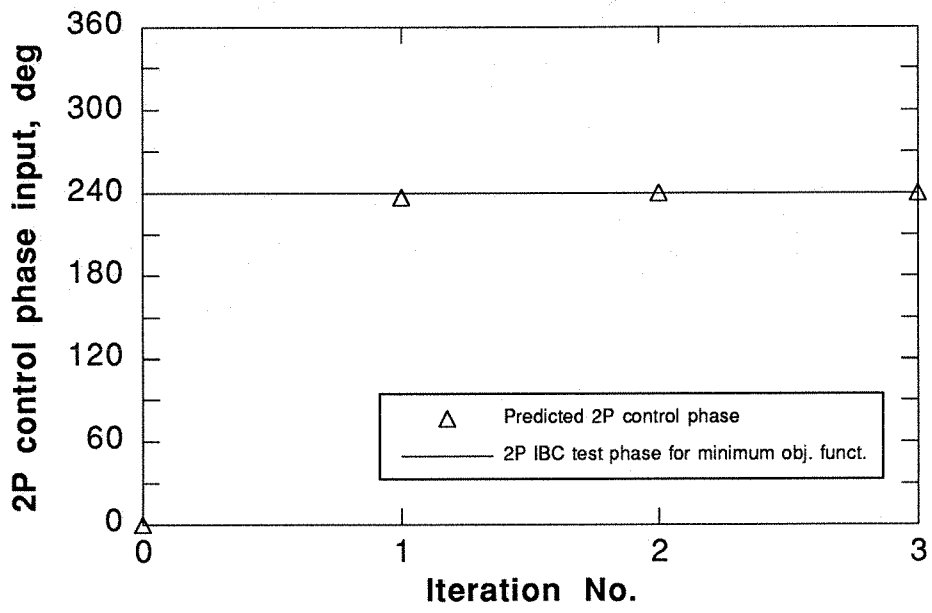

Fig. 8b Case 2 (Noise and Hub Loads Control), convergence of 2P control phase input (simultaneous neural control of noise and hub loads, Fig. 8a shows corresponding objective function).

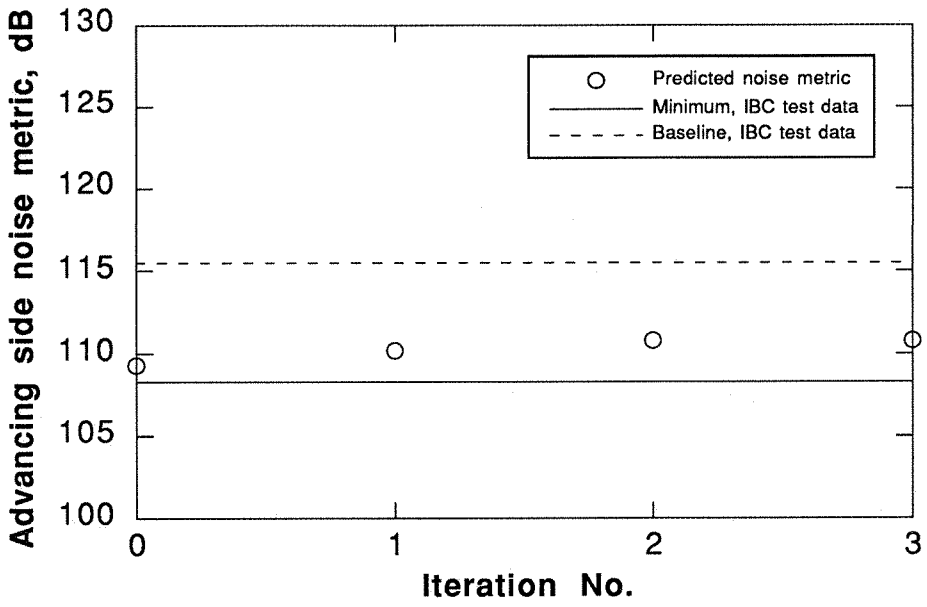

Fig. 9a. Case 2 (Noise and Hub Loads Control), convergence of noise metric ASNM (simultaneous neural control of noise and hub loads).

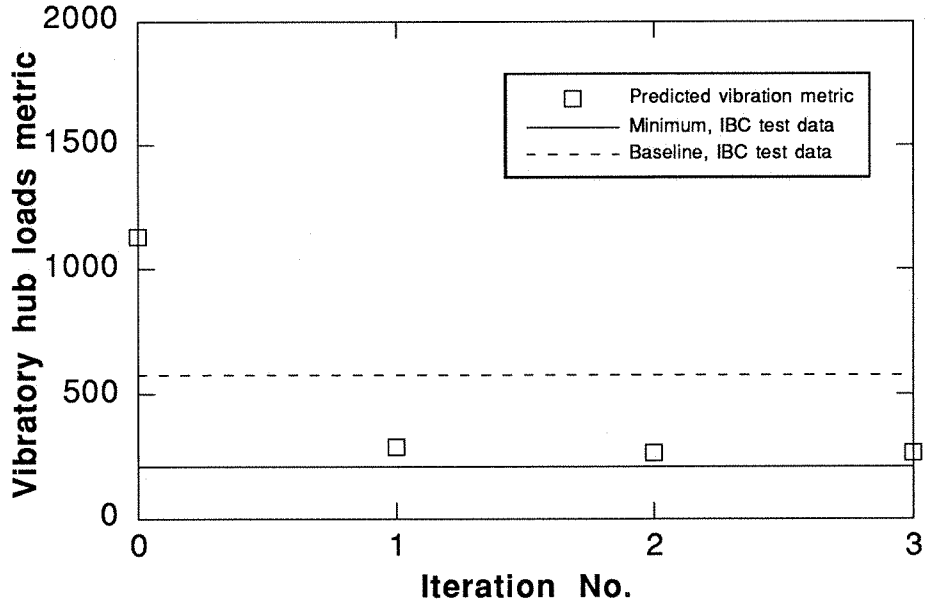

Fig. 9b. Case 2 (Noise and Hub Loads Control), convergence of hub loads metric VHLM (simultaneous neural control of noise and hub loads).

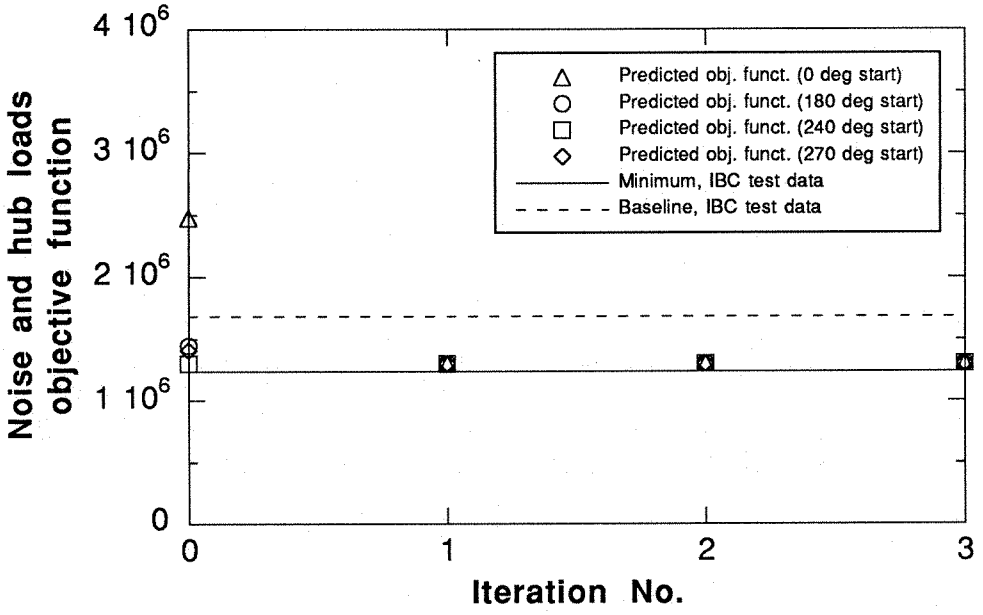

Fig. 10a. Case 3 (Starting Point Sensitivity), convergence of objective function (simultaneous neural control of noise and hub loads).

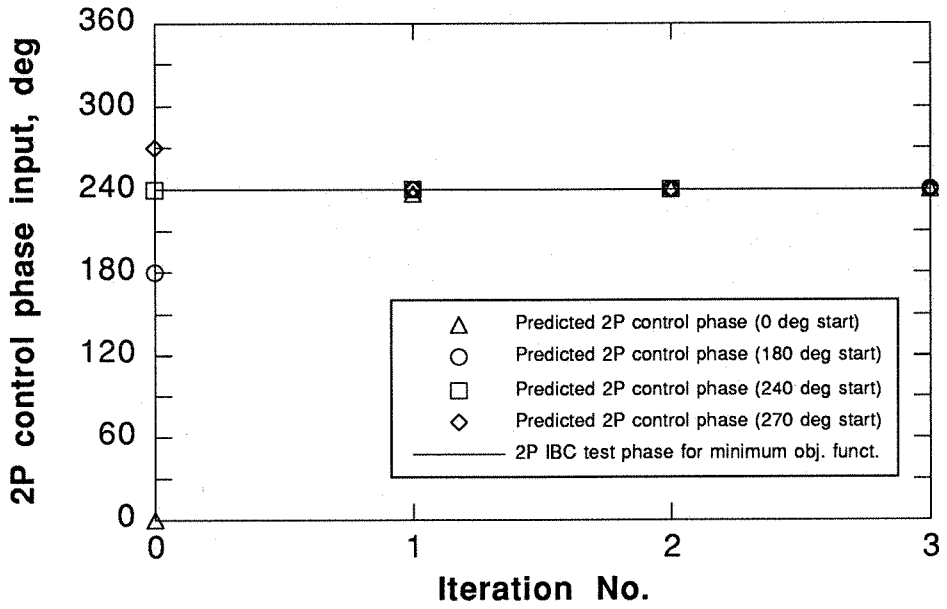

Fig. 10b. Case 3 (Starting Point Sensitivity), convergence of 2P control phase input (simultaneous neural control of noise and hub loads, Fig. 10a shows corresponding objective function).

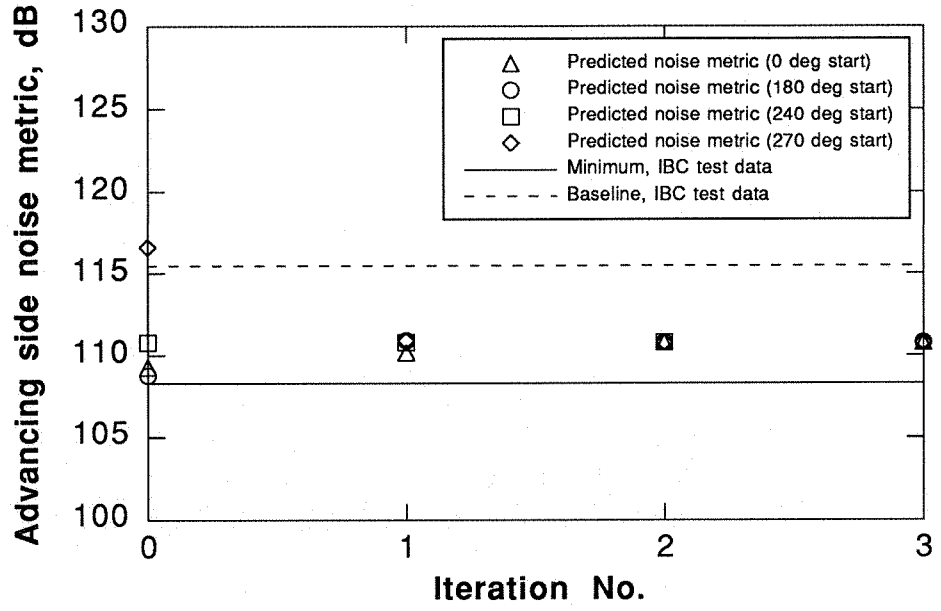

Fig. 11a. Case 3 (Starting Point Sensitivity), convergence of noise metric ASNM (simultaneous neural control of noise and hub loads).

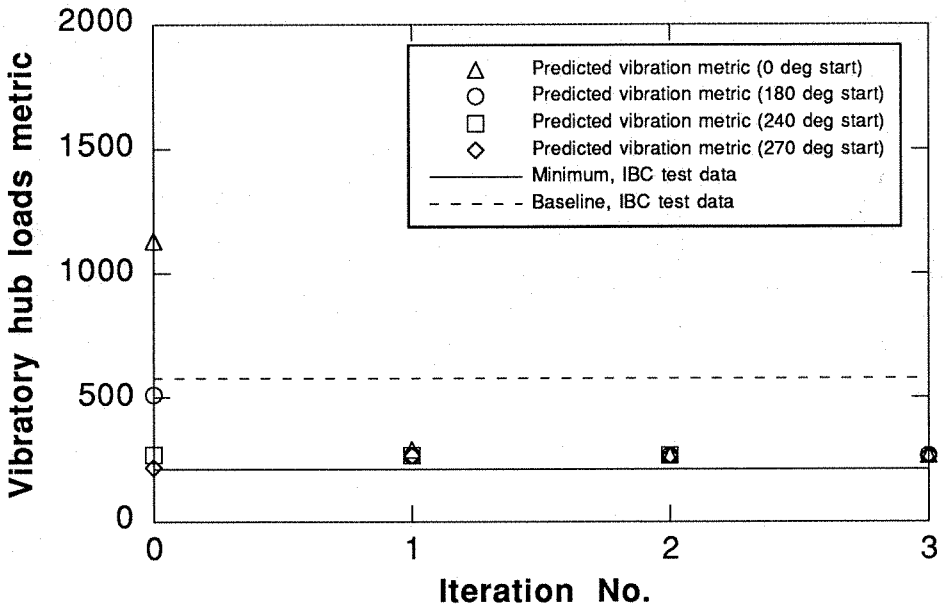

Fig. 11b. Case 3 (Starting Point Sensitivity), convergence of hub loads metric VHLM (simultaneous neural control of noise and hub loads).

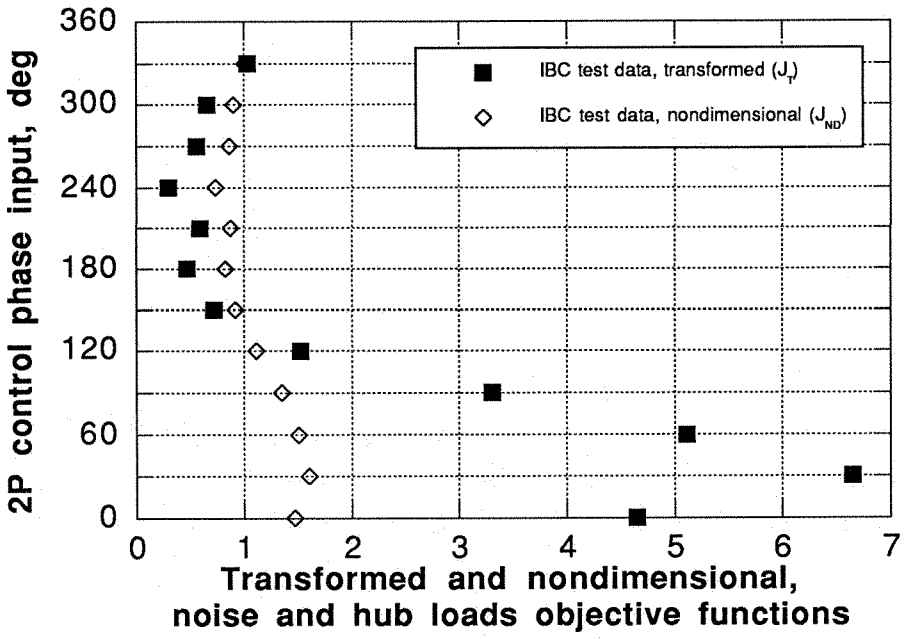

Fig. 12. Case 4 (Reduced Data Base), noise and hub loads objective functions: transformed and nondimensional

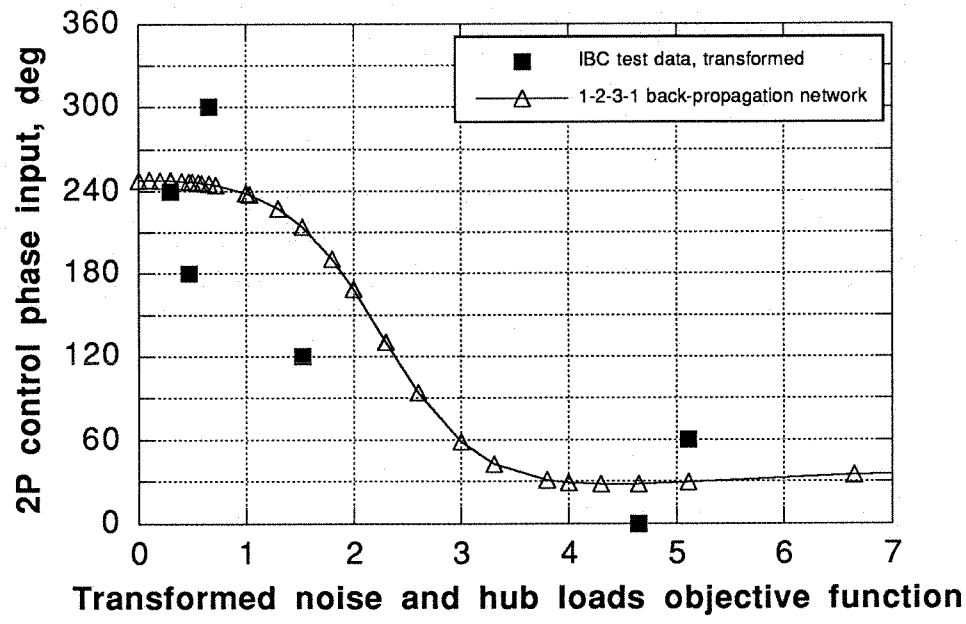

Fig. 13. Case 4A (Odd-Numbered, Six Point Data Base), output of inverted neural network for control, 6 training points.

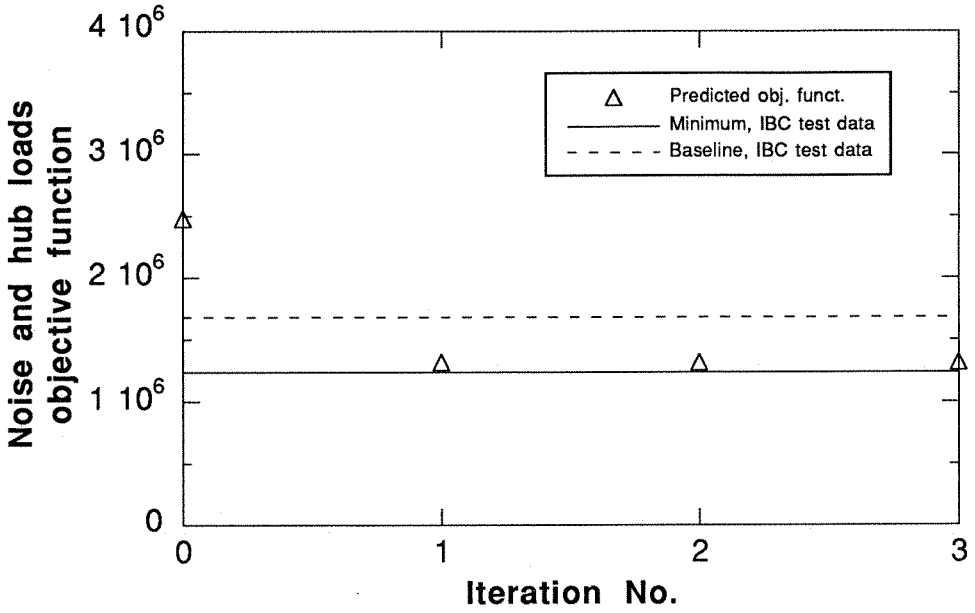

Fig. 14a Case 4A (Odd-Numbered, Six Point Data Base), convergence of objective function J (simultaneous neural control of noise and hub loads).

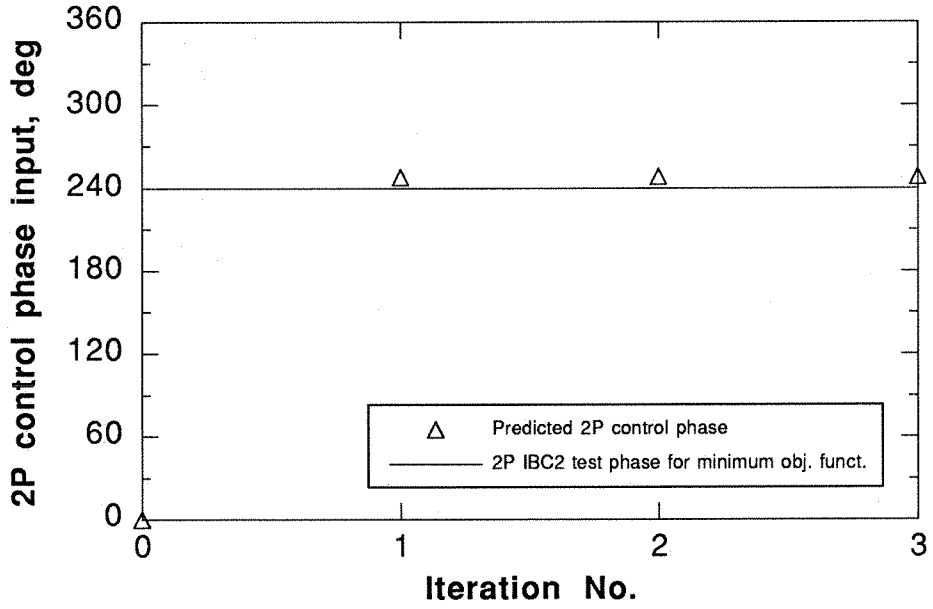

Fig. 14b Case 4A (Odd-Numbered, Six Point Data Base), convergence of 2P control phase input (simultaneous neural control of noise and hub loads, Fig. 14a shows corresponding objective function).

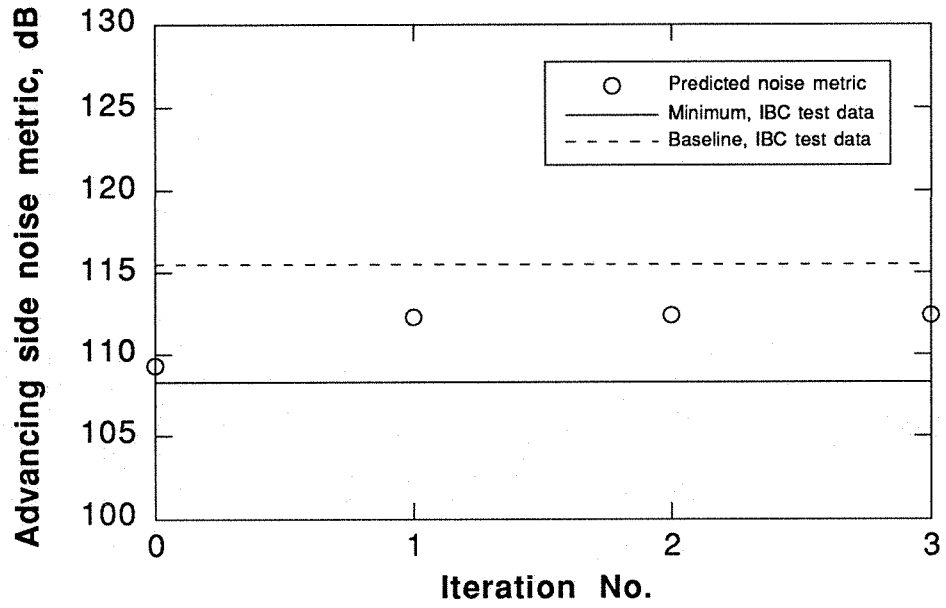

Fig. 15a. Case 4A (Odd-Numbered, Six Point Data Base), convergence of noise metric ASNM simultaneous neural control of noise and hub loads).

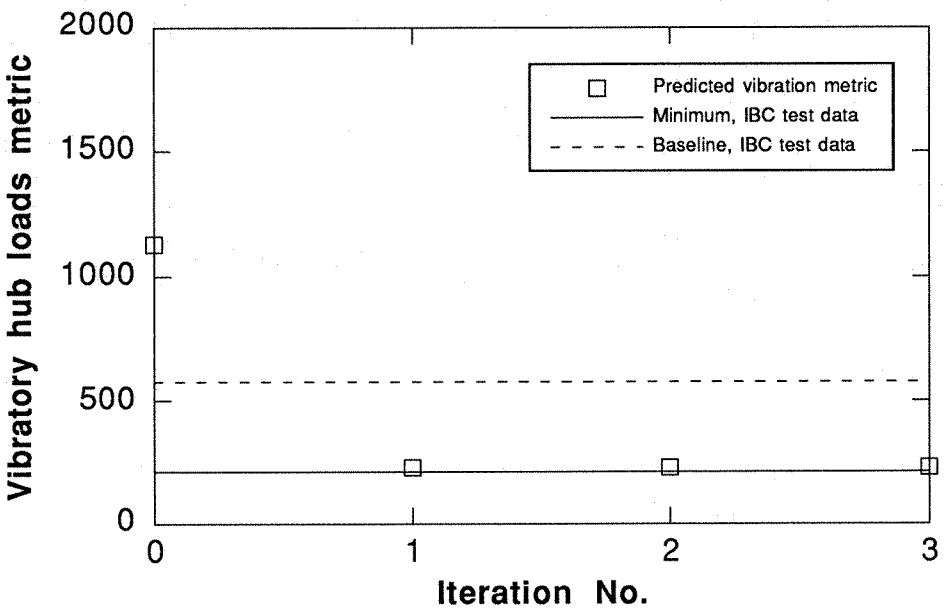

Fig. 15b. Case 4A (Odd-Numbered, Six Point Data Base), convergence of hub loads metric VHLM (simultaneous neural control of noise and hub loads).

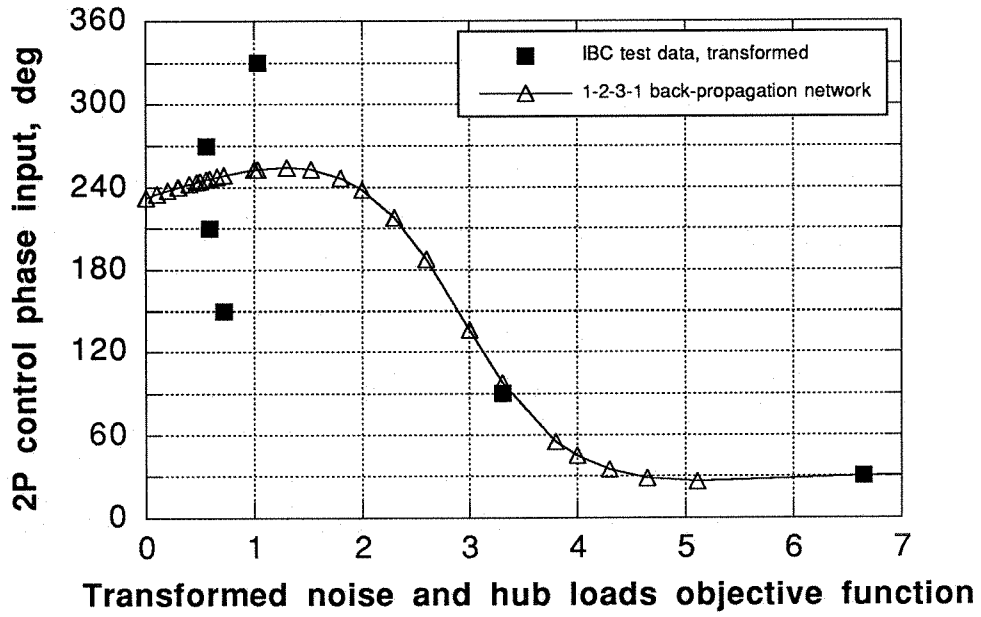

Fig. 16 Case 4B (Even-Numbered, Six Point Data Base), output of inverted neural network for control, 6 training points.

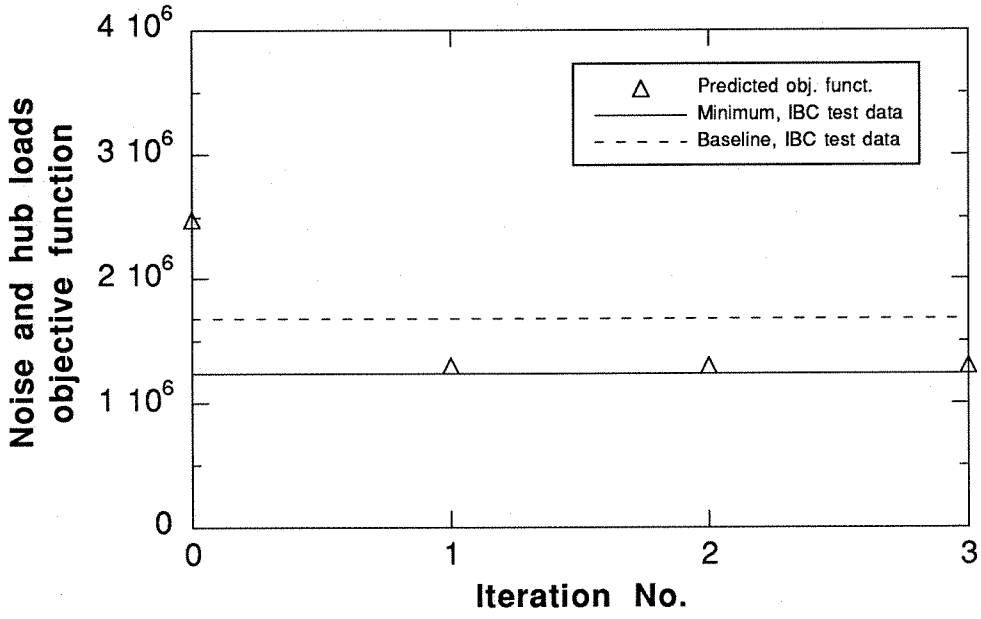

Fig. 17a Case 4B (Even-Numbered, Six Point Data Base), convergence of objective function J (simultaneous neural control of noise and hub loads).

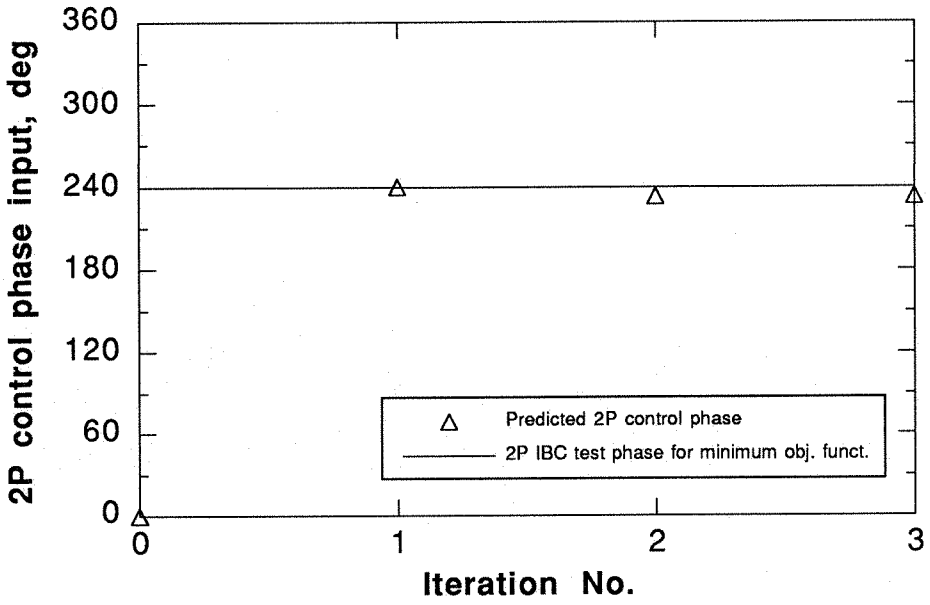

Fig. 17b Case 4B (Even-Numbered, Six Point Data Base), convergence of 2P control phase input (simultaneous neural control of noise and hub loads, Fig. 17a shows corresponding objective function).

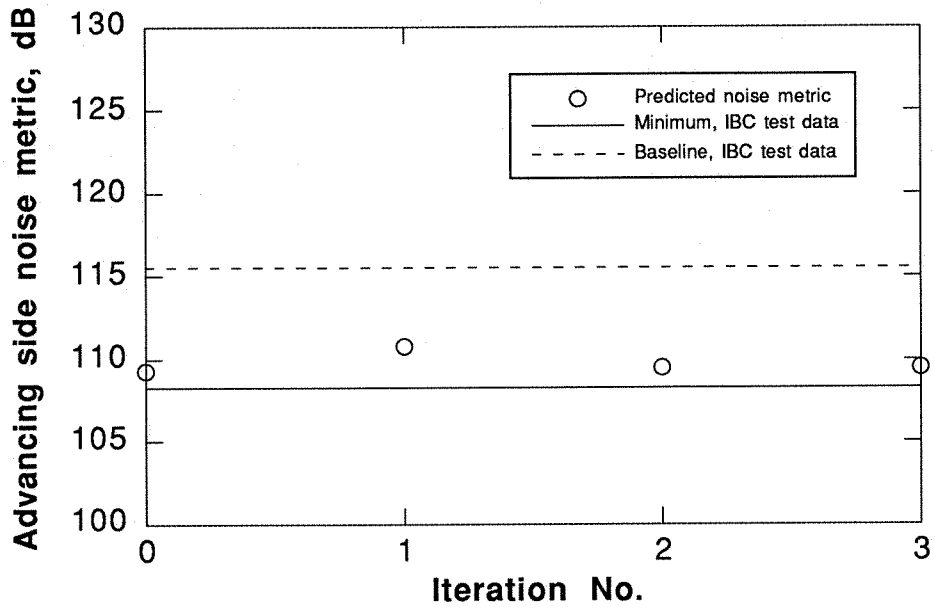

Fig. 18a. Case 4B (Even-Numbered, Six Point Data Base), convergence of noise metric ASNM (simultaneous neural control of noise and hub loads).

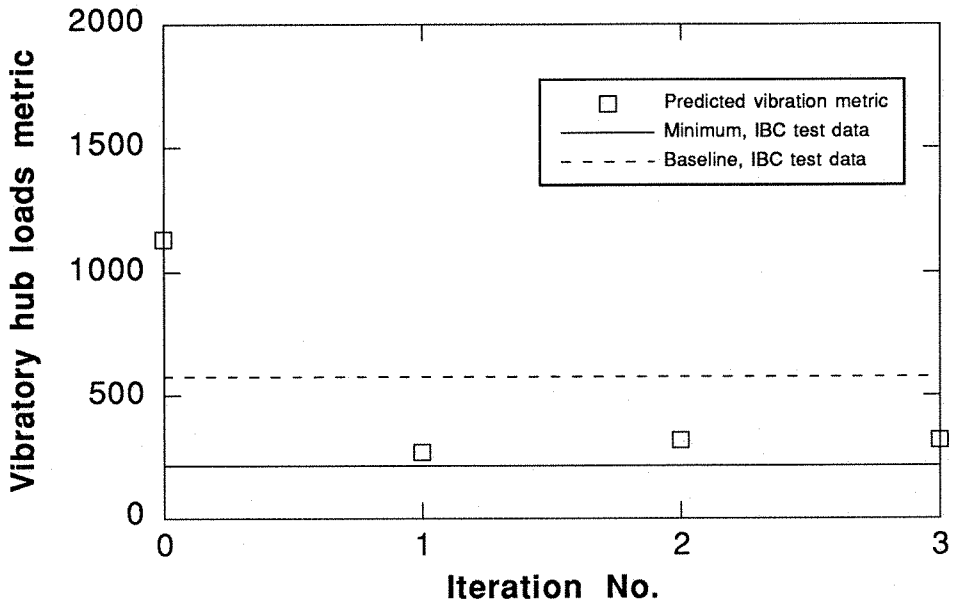

Fig. 18b. Case 4B (Even-Numbered, Six Point Data Base), convergence of hub loads metric VHLM (simultaneous neural control of noise and hub loads).